UPCommons

Portal del coneixement obert de la UPC

http://upcommons.upc.edu/e-prints

Geosynchronous inclined orbits for high-latitude communications

E. Fantino[a], R. M. Flores[b], M. Di Carlo[c], A. Di Salvo[d], E. Cabot[e]

[a]*Space Studies Institute of Catalonia (IEEC), Gran Capitán 2-4, Nexus Building, Office 201, 08034 Barcelona (Spain)*
[b]*International Center for Numerical Methods in Engineering (CIMNE), Polytechnic University of Catalonia (UPC), Building C1, Campus Norte, UPC, Gran Capitán s/n, 08034 Barcelona (Spain)*
[c]*Department of Mechanical and Aerospace Engineering, University of Strathclyde, 75 Montrose Street, Glasgow G1 1XJ (United Kingdom)*
[d]*NEXT Ingegneria dei Sistemi S.p.A., Space Innovation System Unit, Via A. Noale 345/b, 00155 Roma (Italy)*
[e]*School of Industrial, Aeronautical and Audiovisual Engineering (ESEIAAT), Polytechnic University of Catalonia (UPC), Colom 11, 08222 Terrassa (Spain)*

Abstract

We present and discuss a solution to the growing demand for satellite telecommunication coverage in the high-latitude geographical regions (beyond 55°N), where the signal from geostationary satellites is limited or unavailable. We focus on the dynamical issues associated to the design, the coverage, the maintenance and the disposal of a set of orbits selected for the purpose. Specifically, we identify a group of highly inclined, moderately eccentric geosynchronous orbits derived from the Tundra orbit (geosynchronous, eccentric and critically inclined). Continuous coverage can be guaranteed by a constellation of three satellites in equally spaced planes and suitably phased. By means of a high-precision model of the terrestrial gravity field and the relevant environmental perturbations, we study the evolution of these orbits. The effects of the different perturbations on the ground track (which is more important for coverage than the orbital elements themselves) are isolated and analyzed. The physical model and the numerical setup are optimized with respect to computing time and accuracy. We show that, in order to maintain the ground track unchanged, the key

*Corresponding author: elena.fantino@gmail.com (E. Fantino)

parameters are the orbital period and the argument of perigee. Furthermore, corrections to the right ascension of the ascending node are needed in order to preserve the relative orientation of the orbital planes. A station-keeping strategy that minimizes propellant consumption is then devised, and comparisons are made between the cost of a solution based on impulsive maneuvers and one with continuous thrust. Finally, the issue of end-of-life disposal is discussed.

Keywords: Orbits, Geosynchronous, Perturbations, Station-Keeping, Maneuvers, Low-thrust, Disposal, Communications

---

1. Introduction

We present a detailed analysis of a group of geosynchronous, highly inclined orbits for telecommunication satellites. The analysis includes the orbital propagation, a complete station-keeping strategy and an end-of-life disposal plan. The motivations of the study reside in the growing demand for coverage in the high-latitude regions, approximately beyond 55°N. Geostationary (GEO) links work well at low and mid latitudes, with the coverage progressively degrading when moving northwards, for example through Canada, Alaska or the Arctic. The demand for communications service is not limited to land users (television and radio signals, voice and data transmission), but includes aircraft on polar routes, UAVs and maritime navigation. Traditionally, global coverage has been guaranteed by constellations in Low-Earth Orbit (LEO) consisting of many satellites. For example, the Iridium constellation [1] is made up of 66 satellites orbiting at an altitude of approximately 800 km. Classical middle-to-high altitude alternatives are the Molniya and Tundra orbits, with periods of 12 and 24 hours, respectively. Both types are characterized by critical inclination (63.4°) and argument of perigee of 270°, so that the apogee is at high latitudes. The eccentricity is moderate for Tundra (~ 0.26) and high for Molniya (~ 0.75). [2] analyzes the orbital evolution and lifetime of the Russian Molniya satellites. The influence of several perturbing factors on the long-term orbital evolution is found to be related to the choice of the initial value of the right ascension of

the ascending node and the argument of perigee. [3] studies a constellation of satellites in Tundra orbits, and analyzes in detail the effect of each perturbation (Earth's aspheric potential, solar and lunar gravity, solar radiation pressure, atmospheric drag) on the orbital elements. Frozen orbital elements are identified using a double-averaged potential function for the third-body perturbation. This reduces station-keeping costs as far as the eccentricity and argument of perigee are concerned. The maneuver strategy consists in a bang-bang control method. [4] presents the orbital evolution and station-keeping corrections for a geosynchronous polar orbit, called Tundra Polar due to its similarities with the traditional Tundra in terms of orbital period and eccentricity. The orbit is intended to serve mission objectives such as weather monitoring for the North Pole and Canada. The physical model consists of a 12×12 gravity field, solar and lunar gravity and solar radiation pressure perturbations. Thanks to its $90°$ inclination, the Tundra Polar orbit is not affected by the drift of the ascending node due to the second terrestrial zonal harmonic. The orbital parameters are selected so as to limit the variation of the right ascension of the ascending node and the inclination. In this way, only in-plane maneuvers for eccentricity and argument of perigee correction must be implemented. [5] is an extended analysis of satellite constellations for the Arctic communications system. A total of 15 solutions are considered, consisting in inclined, eccentric orbits with periods of 12, 16, 18 and 24 hours, respectively. The assessment is carried out on the basis of coverage, elevation, azimuth, launch cost, radiation exposure and station-keeping requirements. The physical model accounts for the Earth's gravitational potential developed to the second zonal harmonic and an estimation of the effects of the luni-solar third-body perturbations. The study identifies the best solution as that consisting in three satellites in three equally-spaced orbital planes and characterized by a 12 hours period. Other possibilities are the so-called responsive orbits subdivided by [6] into five types: Cobra, Magic, LEO Sun-Synchronous, LEO Fast Access, LEO Repeat Coverage, with periods ranging from typical LEO values (1.5-2 hours) to 8 hours (Cobra orbit) and requiring 6 to 24 satellites operating in different orbital planes. [7] describes the

Wonder orbit, a low-altitude, highly elliptical orbit with critical inclination and designed to obtain a non-drifting repeating ground track. To provide coverage at high latitudes (60°N) with minimum elevations of 35°, a constellation of ten satellites in two planes, with orbital period of 3.4 hours and perigee height of 600 km is suggested. [8] develops an extension of the critical inclination through the application of continuous low-thrust propulsion. The resulting orbit is called Taranis and enables continuous observation of regions beyond 55° latitude using only four spacecraft, and beyond 50° latitude using five spacecraft.

From 2000 to 2015, the Sirius constellation brought digital radio service to high-latitude users in the continental United States and Canada [9, 10]. Satellites Radiosat 1 through Radiosat 3 flew in geosynchronous highly-elliptical orbits with a 23 hours, 56 minutes orbital period (one sidereal day). The elliptical path of this constellation ensured that each satellite spent about 16 hours a day over the continental United States, with at least one satellite over the country at all times. The inclinations ranged from 63.4° to 64.2°. The advantage of a geosynchronous inclined orbit is that its period is equal to that of the Earth's rotation (repetition of orbital pattern), which gives the ground trace a characteristic figure-eight shape centered at the chosen reference longitude. Furthermore, if the orbit is eccentric and the perigee is placed at the point of lowest latitude, the apogee dwell occurs over the northern hemisphere and allows long contacts per orbit of the same satellite with the users. Full coverage is obtained by using three satellites on equally-spaced orbital planes (i.e, at 120° separation, see Fig. 1).

In this contribution, we consider a group of geosynchronous, inclined, eccentric orbits whose orbital elements secure communication service in regions affected by insufficient GEO coverage. This work is a continuation of the study developed in [11]. This paper provides an improved description of the numerical models and algorithms used. A more detailed analysis of the orbital perturbations and station-keeping strategy is presented. Specifically, corrections of the right ascension of the ascending node and their effect on the argument of the perigee are analyzed, both for continuous low-thrust and impulsive maneuvers.

Besides, even though their effect on the ground track is very limited, perturbations of the orbital eccentricity and inclination are also addressed. A section presenting a disposal strategy at end of life concludes the analysis.

The relevance and originality of the present work reside mainly in the treatment of the perturbations, whose degree of approximation is adjusted to the desired accuracy level, and in the station-keeping strategy, which aims at maintaining the ground tracks rather than the orbital elements themselves. **Besides, a procedure has been implemented which uses the coverage requirements and the population distribution in geographical coordinates to limit the number of orbital elements sets to be investigated.** We address the issue of the end-of-life orbit disposal, in observance of the current space regulation against the accumulation of space debris in the more populated orbits.

Section 2 illustrates the criteria adopted for the selection of the orbits. Section 3 describes the physical model, whereas Sect. 4 discusses the simulations setup. The orbital evolution is illustrated in Sect. 5. The station-keeping strategy and the result of its application are explained in Sect. 6. Section 7 illustrates the end-of-life disposal plan. The conclusions are drawn in Sect. 8.

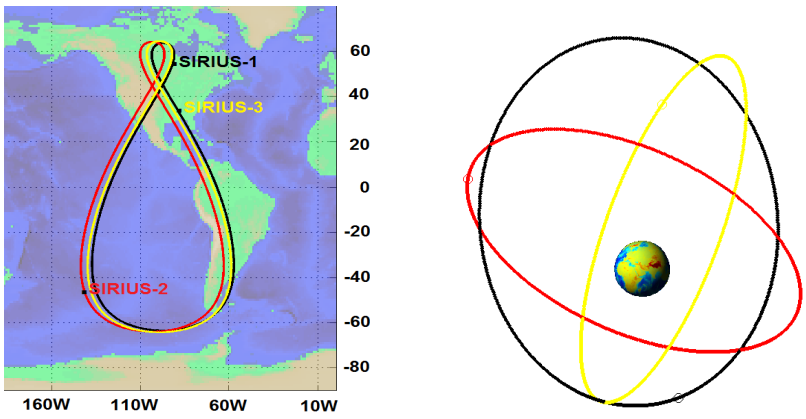

Figure 1: The Sirius constellation: ground track (left) and three-dimensional view of the orbits (right).

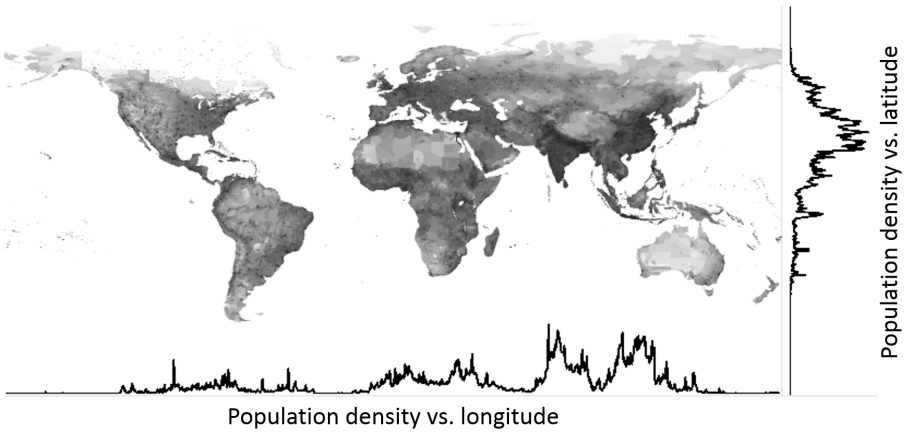

Figure 2: Distribution of world population by latitude and longitude as of 1995 [12, 13].

2. Orbits selection

Following [5] and inspired by the case of the Sirius satellites, we have considered orbits derived from the traditional Tundra. These orbits are geosynchronous, hence their orbital mean motion n_0 is equal to $7.292 \cdot 10^{-5}$ rad/s (i.e., the value of the Earth's sidereal rotation rate). As a consequence, their orbital period T_0 equals 86165.5 s and the semimajor axis a_0 is of 42164.6 km. Furthermore, these orbits are inclined and eccentric. In order to provide service to high-latitude users, the perigee is positioned at the point of lowest latitude, corresponding to an argument of perigee ω_0 of 270°. In this way, the apogee is the point of highest latitude, and the service takes full advantage of the so-called apogee dwell. We have chosen the values of eccentricity e_0 and inclination i_0 which bring satisfactory coverage to select regions, as described here below.

2.1. Coverage analysis: selection of eccentricity and inclination

We have examined the world population distribution in latitude and longitude, and we have identified the most populated areas in the northern hemisphere. According to Fig. 2, such areas are centered in longitude around $\lambda_1 = 100°\text{W}$ (North America), $\lambda_2 = 10°\text{E}$ (Europe) and $\lambda_3 = 100°\text{E}$ (Russia and

China). We have chosen these three values of the longitude as the most economically sensible for operation of a constellation of communication satellites, and we have assessed the coverage provided by constellations of three satellites on geosynchronous orbits with several values of e_0 and i_0. Following the example of the Sirius satellites, we have defined the visibility requirement as a minimum elevation of 60° over the horizon. The three orbital planes are equally spaced and the orbital phases (e.g., the mean anomaly or the true anomaly) of each satellite at the starting time are set by the requirement that the three ground tracks coincide. By tracking the three satellites of the constellation along their orbits, we have mapped the points on the Earth's surface in which the visibility requirement is satisfied by at least one satellite at all times. By trying different combinations of e_0 and i_0, we have identified the values of these two parameters which yield satisfactory coverage over the area of interest. The population distribution diagrams of Fig. 2 indicates scarcity of inhabitants above 55°N, with an extremely small percentage of people living in areas beyond 65°N. Therefore, coverage in regions above this value of the latitude has not been considered as it is not economically justifiable. Moreover, special applications like maritime, aircraft and UAV navigation can be served without the requirement for high elevation angles (tall obstacles blocking the view of the sky are very scarce in the Arctic region). As a result of our assessment, we have identified nine combinations of (e_0, i_0) to use for orbital simulations. These combinations are reported in Table 1, where they are referred to as sets. Initially, in view of the areas to cover, inclinations of 55°, 60°, 65° and 70° were considered. However, it was finally decided to use the critical inclination (63.4°) instead of 65° to allow direct comparisons with the evolution of a classical Tundra orbit. Evenly-spaced values of the eccentricity (0.25, 0.30, 0.35 and 0.40) have been chosen as they make it easier to interpret trends in the data. Coverage maps for each of the nine sets have been determined for each value of the reference longitude (λ_1 to λ_3). A sample of such maps can be found in Figs. 3 and 4.

To each (e_0, i_0) set we have assigned six equally-spaced values for the right ascension of the ascending node Ω_0, namely 0°, 60°, 120°, 180°, 240° and 300°.

Table 1: The nine sets of initial eccentricities e_0 (second column) and inclinations i_0 (third column), and the values $r_{\pi 0}$ (fourth column) and $r_{\alpha 0}$ (fifth column) of the pericenter and apocenter radii of the corresponding geosynchronous Keplerian orbits.

Set	e_0	i_0 (degree)	$r_{\pi 0}$ (km)	$r_{\alpha 0}$ (km)
1	0.25	55.0	31623.5	52705.8
2	0.25	60.0	31623.5	52705.8
3	0.30	60.0	29515.2	54814.0
4	0.25	63.4	31623.5	52705.8
5	0.30	63.4	29515.2	54814.0
6	0.35	63.4	27407.0	56922.2
7	0.40	63.4	25298.8	59030.4
8	0.35	70.0	27407.0	56922.2
9	0.40	70.0	25298.8	59030.4

This results into 54 sets of orbital elements. These are used to initialize the orbit simulations.

3. The physical model

The physical model employed for orbit propagation accounts for the gravitational acceleration due to the terrestrial gravity field, the accelerations caused by the gravity of Moon and Sun as described by [14] (with the positions of the two celestial bodies approximated as in [15, 16]), the effect of the solar radiation pressure (as in [14] with the shadow factor computed according to the double-cone model) and the term associated to the relativistic correction to gravity [17]. The effect of atmospheric drag on the orbit has not been taken into account given the very high perigees (radial distances $> 2.5 \cdot 10^4$ km) of the orbits considered.

As for the terrestrial gravitational acceleration, the traditional

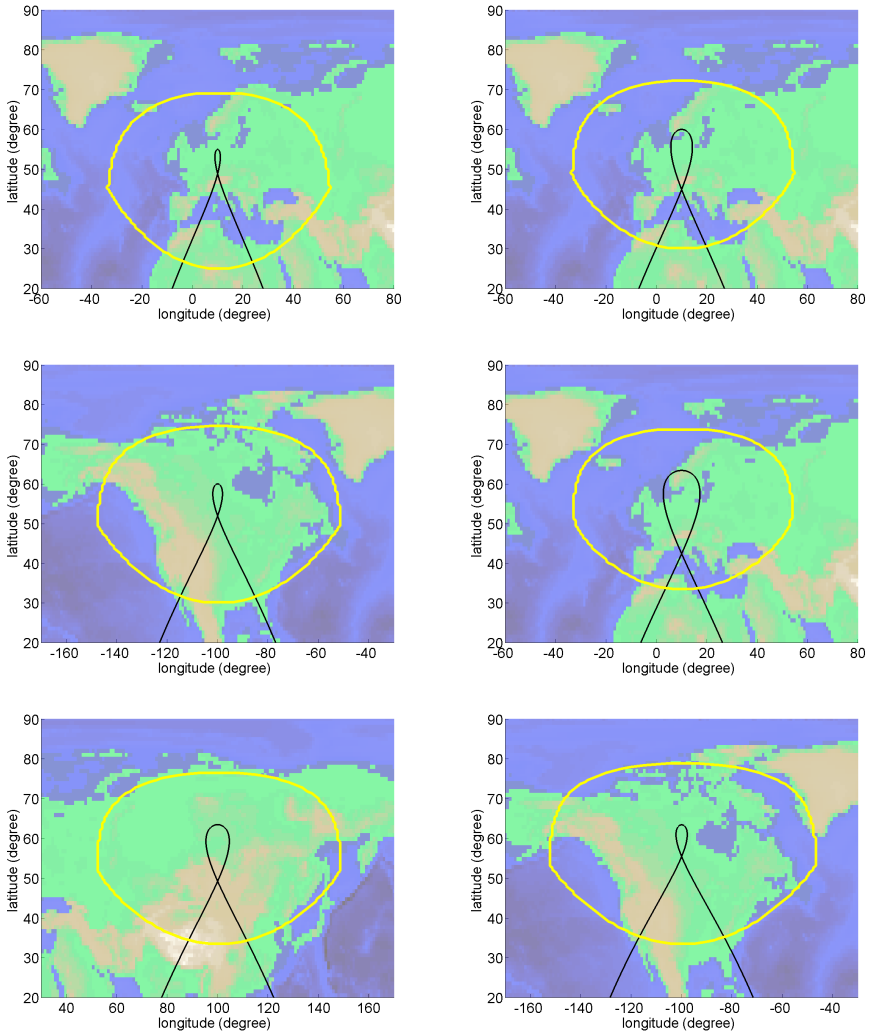

Figure 3: Geographical coverage at 60° minimum elevation for three-satellite constellations based on the orbital parameters of sets 1 (top left), 2 (top right), 3 (middle left), 4 (middle right), 5 (bottom left) and 6 (bottom right), respectively. The ground tracks are centered at the longitudes of interest, i.e., 100°W, 10°E or 100°E.

formulation of the gravitational potential in outer space based on a
165 **spherical harmonic expansion in Associated Legendre Functions [18] has been replaced with a singularity-free representation in Cartesian Earth-fixed coordinates due [19] in which the spherical harmonics are**

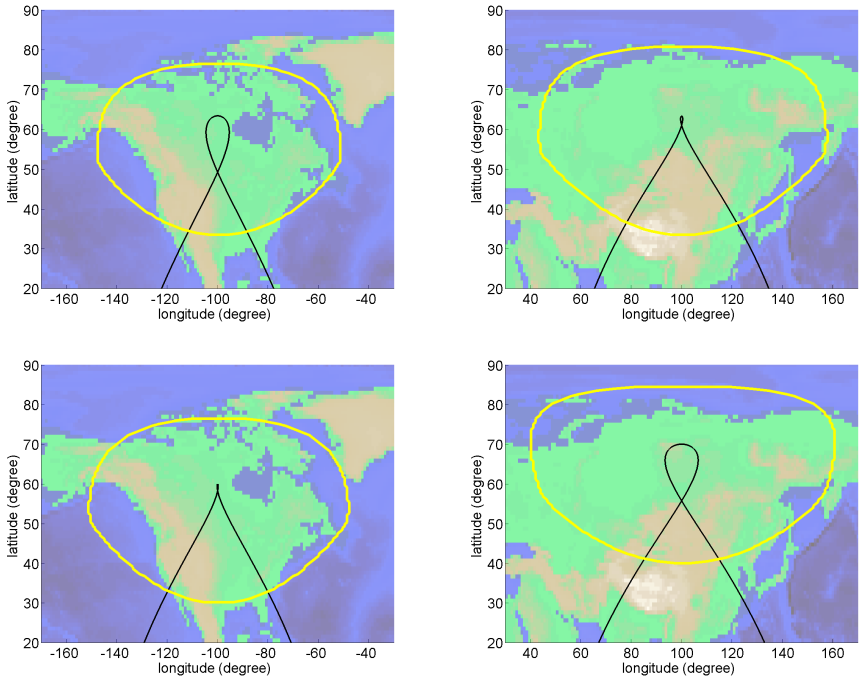

Figure 4: Geographical coverage at 60° minimum elevation for three-satellite constellations based on the orbital parameters of sets 5 (top left), 7 (top right), 8 (bottom left) and 9 (bottom right), respectively. The ground tracks are centered at the longitudes of interest (in this case, 100°W or 100°E).

expressed in terms of Helmholtz polynomials (see [20, 21]). This formulation was improved by [22, 22, 23] with implementation of stable recursion schemes on the Helmholtz polynomials and through the accumulation of so-called lumped coefficients (harmonic sums over the degree), which yields better performance. The adopted geopotential model is the Earth Gravitational Model 2008 [24] in its zero-tide version. It provides the fully-normalized, dimensionless, Stokes coefficients and their associated error standard deviations. The model is complete to degree and order 2159.

4. Numerical setup

The choice of the perturbations to model depends on the level of accuracy sought. For Tundra-like orbits, it has been decided that station-keeping to within 1° accuracy is sufficient for the intended applications. As a matter of fact, a satellite angular displacement of 1° corresponds to a shift in the ground trace of some 100 km. This is a small distance compared to the size of the coverage area (typically several thousand kilometers). This study considers the station-keeping requirements over two years. This time interval is twice the period of the slowest-varying cyclic perturbation (solar), and is thus considered representative of the long-term evolution. To be able to sense 1° errors in position after two years, the discretization error of the orbit propagator must be small compared with this value. A uniform drift of 1° over two years is equivalent to 0.0014° per orbit (i.e., per sidereal day). Given the altitude of the orbits under study (the lowest perigee height is of 19000 km, approximately), this corresponds to a distance of more than 600 m per orbit. Therefore, the error in the trajectory propagation must be at least 10 times smaller, i.e., 60 m/orbit. We set a conservative value of 40 m/orbit. The propagator tolerance and time step must be chosen so as to respect the target accuracy. It has been determined through numerical experiments that using a relative tolerance of 10^{-6} and a maximum time step of 600 s produces errors well below the required 40 m/orbit threshold. The required accuracy also determines the magnitude of the perturbing forces to consider. A constant acceleration of 10^{-8} m/s^2 acting for one day (the orbital period) causes a drift of 40 m. This means that perturbing accelerations below such value can be neglected without altering the quality of the results. Note also that most perturbations are likely to oscillate along the orbit instead of remaining constant, so their cumulative effect will be smaller (this is a worst-case scenario estimate). According to this criterion, the perturbations due to atmospheric drag and relativistic corrections (close to 10^{-9}m/s^2) can be ignored as they fall well below the 10^{-8} m/s^2 level. For standard communication satellites with an area-to-mass ratio of 0.01 m^2/kg, the

effect of solar radiation pressure in these orbits yields accelerations below 10^{-7} m/s^2, which is barely appreciable and with a marginal effect on the station-keeping requirements.

4.1. Choice of the expansion degree of the geopotential

When performing the harmonic synthesis of the geopotential and its first-order gradient, the number of spherical harmonics to retain (i.e., the expansion degree) is determined by the accuracy requirement. Given that higher-order harmonics decay rapidly with altitude, the expansion degree necessary to meet the target accuracy decreases with height. To make the computations as efficient as possible, the number of degrees to retain must be determined dynamically while the trajectory is being computed. To determine the optimum expansion degree at each altitude, a sample of 36 longitudes and 17 latitudes has been analyzed (corresponding to points spaced 10° along a sphere). The expansion degree required to reduce the truncation error below 10^{-8}m/s^2 for all the points of the grid has been determined, i.e., the degree for which the difference between the complete EGM2008 model and the truncated series is less than the threshold acceleration. This procedure has been repeated for several altitudes in geometric series with ratio 2 starting at an altitude of 250 km and covering the complete trajectory envelope. The table containing the required expansion degree as a function of altitude is used by the numerical integrator to compute the gravitational acceleration, guaranteeing the required accuracy while keeping the computational cost to a minimum (Fig. 5).

5. Simulations

The physical model has been coded in Fortran. The executable has been called CHEOPs which stands for Cartesian Harmonic synthEsis Orbit Propagator. CHEOPs incorporates a 7(8) Runge-Kutta-Fehlberg numerical integrator.

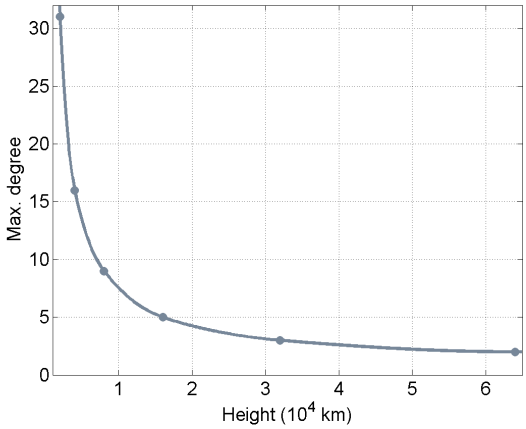

Figure 5: Expansion degree required to achieve the target accuracy for each height.

5.1. Preprocessing: removal of the linear drift of the ascending node due to J_2

It is well known (see e.g. [25] p. 347) that the longitude of the ascending node drifts at a uniform rate due to the second zonal harmonic J_2 (0.0010826) of the terrestrial gravity field. Due to this effect, the orbital plane of the satellite precesses at a rate given by

$$\dot{\Omega}_{J2} = -\frac{3}{2}\left(\frac{R_E}{a_0}\right)^2 \frac{n_0 J_2 \cos i_0}{(1-e_0^2)^2}, \tag{1}$$

which, in turn, would cause the ground track to move eastwards at the same rate. On the other hand, the ground track of a Keplerian orbit with a slightly different mean motion n would move to the East at a rate $n - n_0$. Thus, the eastwards drift of the ground track due to J_2 can be countered by changing the period of the (originally) geosynchronous orbit in such a way that both effects cancel out. That is,

$$n = n_0 - \dot{\Omega}_{J2}. \tag{2}$$

Note that Eq. 2 assumes the change in orbital period is small, so there is no need to modify the rate of precession given by Eq. 1. Once the required period of the orbit $T = 2\pi/n$ has been determined, the initial conditions for the orbit propagator must be obtained. Given that the real orbit is not Keplerian, the

semimajor axis cannot be computed directly from Kepler's third law. Defining T as the time between passages through the ascending node, its value can only be determined after a set of initial conditions has been chosen and the orbit has been numerically propagated. Therefore, the initial conditions must be determined iteratively. From Kepler's third law we can derive the approximate variation δT of period that corresponds to a given change δa in semimajor axis:

$$\delta T \approx \frac{6\pi^2}{GM_E}\frac{a^2}{T}\delta a. \tag{3}$$

Starting with an approximation of the semimajor axis a_i, an improved estimate a_{i+1} can be obtained by combining Eqs.2-3:

$$\frac{2\pi}{n_0 - \dot{\Omega}_{J2}} = T_i + \frac{6\pi^2}{GM_E}\frac{a_i^2}{T_i}(a_{i+1} - a_i), \tag{4}$$

leading to the following iterative formula:

$$a_{i+1} = a_i + \left(\frac{2\pi}{n_0 - \dot{\Omega}_{J2}} - T_i\right)\frac{GM_E}{6\pi^2}\frac{T_i}{a_i^2}. \tag{5}$$

For all the orbits tested, the change in period respect to the ideal geosynchronous case, $\Delta T = T - T_0$, amounts to just a few seconds. Therefore, the approximation made in Eq. 2 is acceptable.

5.2. Orbital evolution

The 54 sets of initial conditions presented in Sect. 2 have been propagated over intervals of two years, to encompass all the cycles present in the model. Due to the high altitudes of these orbits, the code automatically sets the expansion degree to 4 or less (see also Fig. 5). The evolution of the orbits under the forces accounted for in the model is summarized in Table 2, which provides the maximum and typical variation of the orbital parameters of interest as well as a reference (i.e., the set and the initial value of the right ascension of the ascending node) to the representative orbit for each case. The orbital parameters given are the eccentricity e, inclination i, argument of perigee ω, right ascension Ω of the ascending node, and the longitude LAN of the ascending node, which measures the East-West (E-W) motion of the ground track. Note that the semimajor

Table 2: Maximum and typical variation of the orbital parameters of interest and a reference (i.e., the set and the initial value of the right ascension of the ascending node) to the representative orbit for each case.

Element	Maximum var.	Set	Ω_0	Typical var.	Set	Ω_0
e	0.07	9	120°	0.03	5	60°
i	1.2°	1	300°	0.5°	4	120°
ω	15°	9	180°	6°	8	0°
Ω	11°	7	0°	9°	6	300°
LAN	150°	1	60°	100°	4	300°

axis is not shown because it is related to the orbital period, so its effect is lumped into LAN, i.e., in the loss of synchronism with respect to the rotation of the Earth. Figures 6 illustrates the evolution of e, i, ω and LAN for the most representative cases of the table, i.e., sets 1 and 9, with the six values of Ω_0. The evolution of Ω for the worst case (set 7) and for a typical case (set 6) is given in Fig. 7. The most important secular perturbation is due to the Moon, which causes variations of the orbital period which in turn move the ground track in the E-W direction. The displacement can reach hundreds of degrees over a two-year span and needs a major axis correction in order to keep the ground track fixed. On the other hand, the fluctuations of eccentricity and inclination have a very limited effect on the ground track and do not require correction over a two-year period (as far as the ground track is concerned). The maximum drift of the argument of perigee observed is around 15° over two years and needs to be periodically corrected.

6. Station keeping

Two different station-keeping strategies are devised. A classical one relying on impulsive maneuvers, and another suitable for electric propulsion with the corrections applied over thrust arcs spanning an important fraction of the orbital period. To determine the details of the low-thrust maneuvers (including

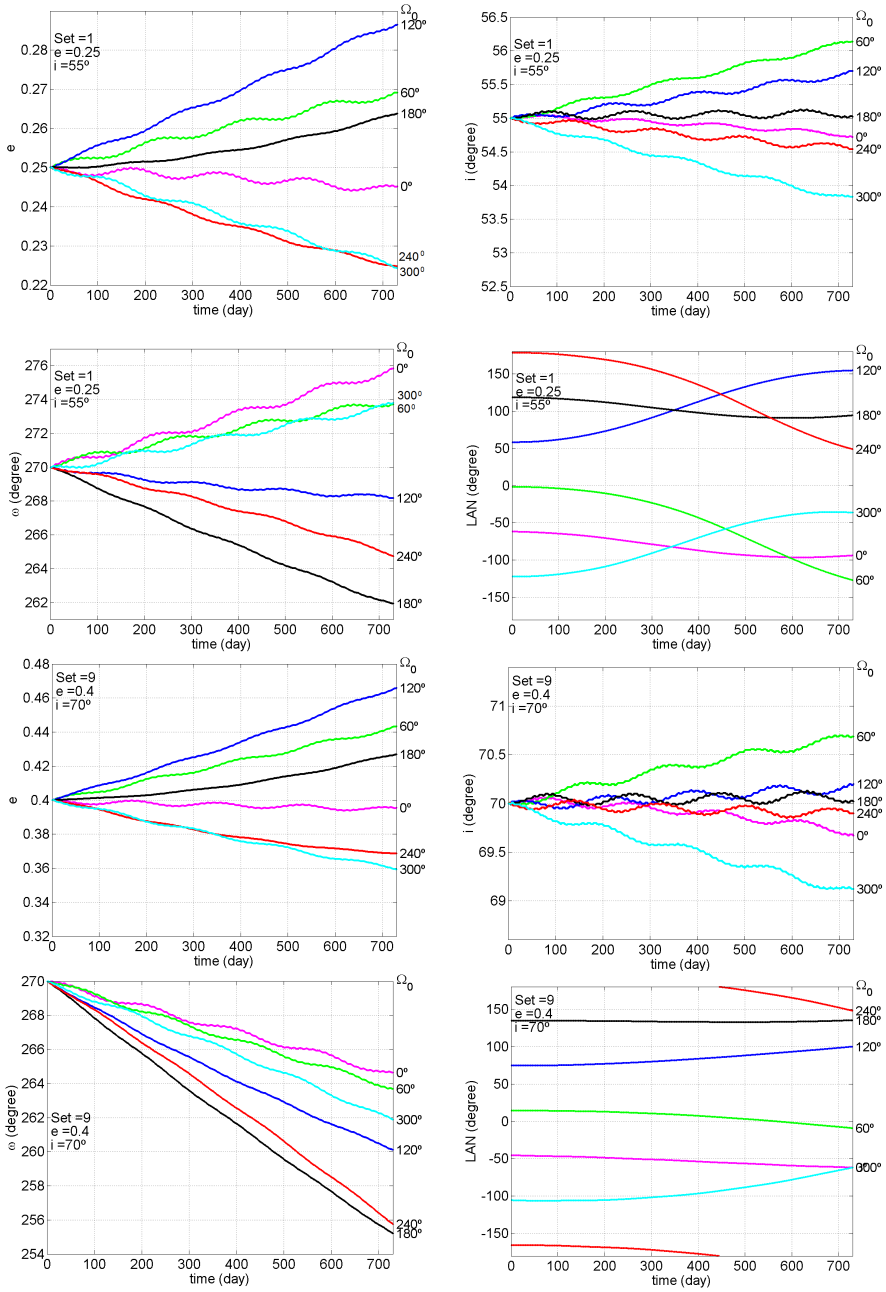

Figure 6: Evolution of the relevant orbital parameters of the orbits of sets 1 and 9: eccentricity e, inclination i, argument of perigee ω, longitude of the ascending node LAN.

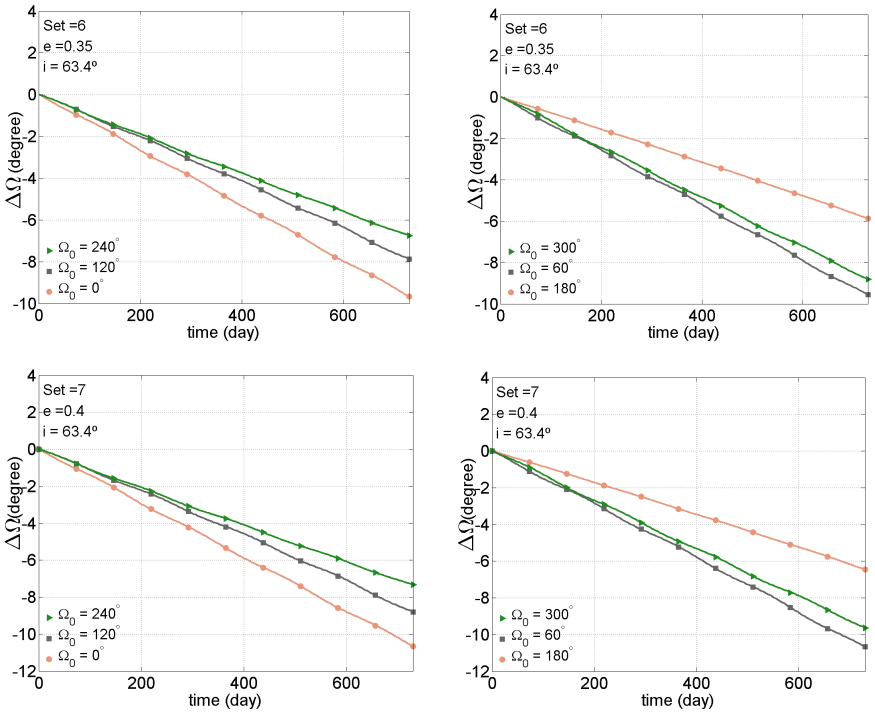

Figure 7: Drift of the ascending node: sets 6 (top) and 7 (bottom).

duration) the value of the acceleration of the spacecraft is needed. This, in turn, requires knowledge of the vehicle mass and the thrust available. An initial spacecraft mass of 3000 kg and maximum thrust of 79 mN have been assumed in this study yielding an acceleration of $2.63 \cdot 10^{-5}$ m/s^2. The maximum available acceleration increases as propellant is consumed (assuming no degradation of the propulsion system). However, the acceleration has been taken equal to the initial value at all times, which is a conservative assumption. This simplifies greatly the interpretation of the charts relating the length of the thrust arcs to the change in orbital elements. Moreover, the mass fraction of propellant in a spacecraft using electric thrusters is likely small, reducing the changes in acceleration. The duration of the thrust arcs can be of several hours and may require changes in spacecraft attitude. Therefore, to avoid disrupting normal satellite operations, it has been assumed that all low-thrust maneuvers are applied near the perigee (where the satellite does not provide coverage and can thus be safely taken offline).

6.1. Correction of the longitude of the ascending node

It is important to realize that from the point of view of operation, the position of the orbital plane is of minor importance compared with the correct placement of the ground track. The orbital perturbations cause the right ascension of the ascending node to change and therefore affect the E-W position of the ground track. However, this effect is very small compared with the changes caused by fluctuations of the orbital period. If the orbital period **of a geosynchronous orbit** were to change by ΔT for any reason, this would cause a drift ΔLAN of the longitude of the ascending node,

$$\Delta\text{LAN} = -360 \left(\frac{\Delta T}{T_0} \right) \text{ degrees per orbit.} \tag{6}$$

The magnitude of this drift is so important that it overshadows the effect of the orbital plane precession. Therefore, the station-keeping strategy must focus on adjusting the orbital period to keep the ground track in place. Any E-W drift of the ground track caused by the different perturbations is countered by

introducing an appropriate change in the orbital period. This is achieved with a two-burn maneuver which changes the semi-major axis while keeping the other orbital elements unchanged. The first burn takes place at the perigee of the initial orbit and the second at the apogee of the final orbit. From Kepler's third law, the variation Δa in semimajor axis needed to change the orbital period by a small amount ΔT is

$$\Delta a = \frac{T_0 G M_E}{6\pi^2 a^2} \Delta T. \tag{7}$$

The impulse for the two-burn maneuver can be linearized (assuming small changes in velocity) yielding:

$$\Delta V = \frac{G M_E}{4a^2} \left(\frac{1+e}{V_\pi} + \frac{1-e}{V_\alpha} \right) \Delta a. \tag{8}$$

where V_π and V_α denote the perigee and apogee velocities, respectively. Using Eqs. 7 and 8, the cost of the period control maneuver can be determined. For the cases under study the fluctuations in orbital period are very small (35 s over two years for the worst-case scenario, set 1, $\Omega_0 = 60°$). A change of orbital period of 35 s can be accomplished with an impulse $\Delta V^I_{\mathrm{LAN}}$ of just 0.22 m/s. Therefore, the contribution to the overall impulse budget (totaling hundreds of m/s) can be safely neglected.

6.2. Correction of the right ascension of the ascending node

The motion of the ascending node is mostly due to lunisolar perturbations, with the Moon accounting for roughly two thirds of the drift observed. Furthermore, numerical experiments show that the effect depends on the inclination of the satellite orbit relative to the orbital plane of the Moon. The drift of the ascending node is fastest when both orbits are almost coplanar and vanishes when they are perpendicular. At the epoch of the start of the simulations (July 1^{st} 2013), the ascending node of the lunar orbit has a right ascension of 5° and an inclination of 28° respect to the equator. The minimum relative orbital inclination (satellite respect to Moon) is obtained when the ascending nodes of the Moon and satellite coincide. Therefore, the orbital planes needing the largest Ω correction are those with $\Omega_0 = 0°$ and 60°.

As stated in the previous section, the E-W position of the orbital plane has a minor effect on the position of the ground track, which is controlled through very small adjustments of the orbital period. However, in order to have a properly working constellation, a 120° spacing between the orbital planes must be maintained. To optimize the propellant consumption, it was decided to correct only the drift $\hat{\Omega}$ of each orbital plane with respect to the mean motion of the constellation. Let $\Delta\tilde{\Omega}$ be the mean change in Ω of the constellation:

$$\Delta\tilde{\Omega} = \frac{1}{3}\sum_{i=1}^{3}\Delta\Omega_i. \tag{9}$$

Here, Ω_i denotes the right ascension of the ascending node of plane i and $\Delta\Omega_i$ its variation. The station keeping maneuvers are designed to correct the change in $\hat{\Omega}$, defined as

$$\Delta\hat{\Omega}_i = \Delta\Omega_i - \Delta\tilde{\Omega}. \tag{10}$$

By removing the mean drift of the constellation, the cost of the station-keeping maneuvers is reduced compared to a simpler strategy based in controlling each orbital plane independently. To illustrate the gain obtained with this strategy, Fig. 8 depicts the evolution of $\hat{\Omega}$ for typical (set 3) and worst-case scenarios (set 9). While, as shown in Table 2, the maximum change in Ω over 2 years is 11° (set 7, $\Omega_0 = 0°$), the largest change in $\hat{\Omega}$ is just 3° (set 9, $\Omega_0 = 180°$). That is, the impulse budget is cut down by 70%. The typical correction, on the other hand, is reduced from 9° to just 1° (a 90% decrease).

6.2.1. Impulsive maneuver

When the perigee argument is 90° or 270° and in the limit of small corrections, the change in Ω is achieved with a single burn near the apogee or perigee which rotates the velocity vector by an angle γ [26, 27]:

$$\gamma \approx \Delta\Omega \sin i. \tag{11}$$

Note that the expression above is only valid if $\Delta\Omega \ll 1$ rad. Given that the magnitude of the impulse is proportional to the satellite velocity at the time of

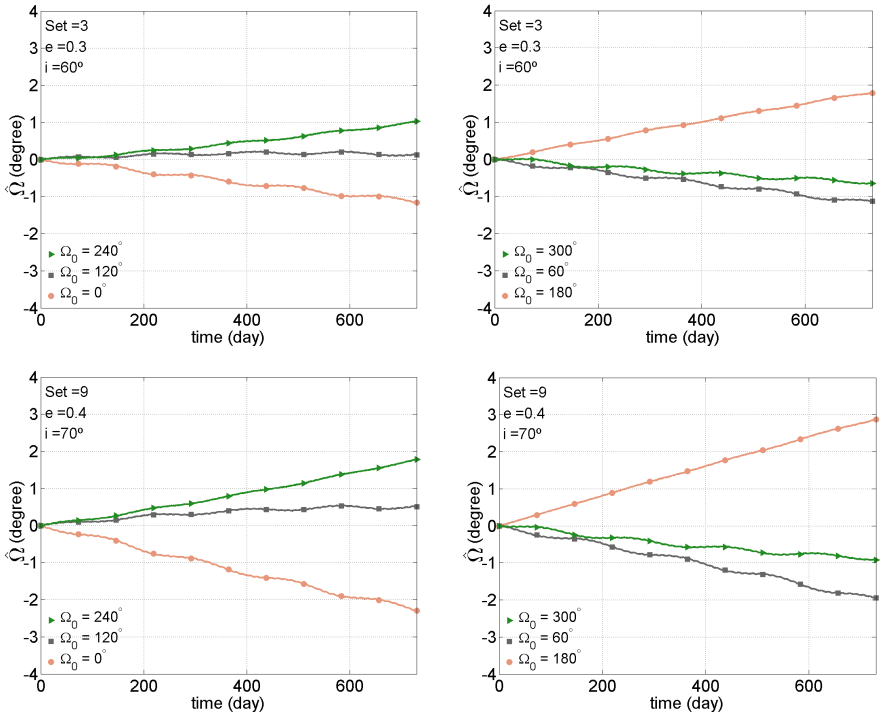

Figure 8: Drift of $\hat{\Omega}$: sets 3 (top) and 9 (bottom).

the burn, it is preferable to apply the maneuver at the apogee. The impulse needed is then:

$$\Delta V \approx V\gamma \approx V_\alpha \Delta\Omega \sin i, \tag{12}$$

where small angles are assumed. For the orbits under consideration, the typical magnitude of the impulse is 34 m/s for each degree of correction. For a worst-case scenario of 3° Ω correction over two years (set 9, $\Omega_0 = 180°$), the total impulse ΔV_Ω^I is 100 m/s. It is worth noting that this maneuver causes a change in argument of perigee as a side effect. For a burn near the apogee, the variation in ω is approximately

$$\Delta\omega \approx \Delta\Omega \cos i. \tag{13}$$

This, depending on the sign of the relevant terms, reduces or increases the correction of the argument of perigee needed to compensate orbital perturbations. Given that the signs change for different orbits of the same set, the next section (correction of ω) assumes a worst-case scenario to obtain a conservative estimate of the impulse budget (i.e., the magnitude of the correction is always increased).

6.2.2. Low-thrust maneuver

To change the ascending node, thrust must be applied perpendicular to the orbital plane [25]. Following [28] and denoting with f the magnitude of the acceleration imparted by the motor, the execution of thrust arcs symmetric with respect to the perigee yields a variation in Ω

$$\Delta\Omega = -\frac{a^2 f}{GM_E\sqrt{1-e^2}\sin i}\left(-3e\bar{E} + 2\sin\bar{E} + 2e^2\sin\bar{E} - \frac{1}{2}e\sin 2\bar{E}\right). \tag{14}$$

As usual, a, e and i are semimajor axis, eccentricity and inclination (all left constant by the maneuver), whereas $\bar{E}$ is the half-span of the thrust arc (measured in terms of eccentric anomaly). If β denotes the thrust elevation over the orbital plane, then for a positive change in Ω the thrust vector must be antiparallel ($\beta = -90°$) to the orbital angular momentum when the satellite is in the southern hemisphere and parallel ($\beta = +90°$) in the remaining part of the orbit. Figure 9 (right) shows the change in Ω per orbit achieved as a function

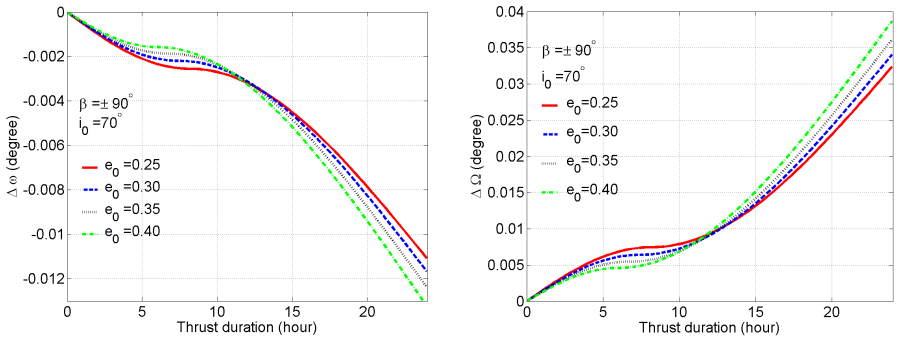

Figure 9: Right: change in Ω per orbit achieved as a function of the eccentricity and total duration of the thrust arc for an orbit with 70° inclination by thrusting perpendicular to the orbital plane. Left: effect of the maneuver on the argument of perigee ω.

of the eccentricity and total duration of the thrust arc for an orbit with 70° inclination. The thrust arc is symmetric with respect to the perigee. So, for example, a total duration of 10 hours corresponds to an arc spanning from 5 hours before perigee to 5 hours after perigee. Note that the curves show a point of zero slope. This happens when the satellite crosses the Equator, causing the net torque with respect to the line of nodes to vanish. Therefore, care must be taken not to apply the maneuver close to the nodes, as it would waste propellant. As was the case for the impulsive maneuver, there is a change in argument of the perigee associated with the correction of Ω:

$$\Delta\omega = -\frac{f}{\cot i}\sqrt{1-e^2}\left(-3e\bar{E} + 2\sin\bar{E} + 2e^2\sin\bar{E} - \frac{1}{2}e\sin 2\bar{E}\right). \qquad (15)$$

The magnitude of the coupling is depicted on the left graph of Fig. 9. For a worst-case scenario of 3° Ω correction over two years for the most eccentric orbit (set 9, $\Omega_0 = 180°$), the correction per orbit is 0.0041°. A thrust arc of 4.2 hours is required with an associated change in ω of 0.0014° per orbit (1° over two years). Note that the duration of the arc is within the acceptable range, as it takes place in the area where the slope of the curves is large (i.e., the satellite is far enough from the Equator). The total impulse is computed as the product of the spacecraft acceleration times the duration of the thrust arc. This yields a change in velocity of 0.4 m/s per orbit or $\Delta V_\Omega^{LT} = 290$ m/s over two years.

6.3. Correction of the argument of perigee drift

Computations show that, for the worst-case scenario, roughly 20% of the perigee drift is due to the harmonics of Earth's gravitational field, 25% is caused by the Sun and 55% by the Moon. In classical Molniya orbits the critical inclination is used to minimize changes in ω due to J_2. For Tundra-like orbits, however, the choice of inclination affects the precession of the perigee to a much lesser extent. This is due to the perturbations caused by the non-spherical Earth decaying rapidly with altitude. As was the case with the ascending node, lunar perturbations depend on the relative orientation of the satellite and Moon orbits (i.e., the right ascension of the ascending node). In this case, however, the effect is maximum for the orbital planes with ascending nodes opposite to the Moon (i.e., 180° and 240°).

6.3.1. Impulsive maneuver

To carry out an in-plane rotation of the major axis of the orbit, an optimized impulsive two-burn maneuver has been used. It involves an elliptical transfer orbit with the major axis oriented halfway between the initial and final orbits [29]. Due to the symmetry of the problem, the two burns have the same magnitude. The transfer has two degrees of freedom, the eccentricity of the transfer orbit and the true anomaly of the first burn. These must be determined by minimizing the total impulse. As the optimization method described in the reference is very cumbersome to implement in software, an alternative, more computer-friendly strategy has been developed. The optimum combination is determined with a two-stage algorithm. For a given value θ of the true anomaly of the first burn, the eccentricity $e^\star$ of the transfer orbit yielding the minimum impulse can be found by solving the equation

$$\frac{\partial \Delta V(e^\star, \theta)}{\partial e^\star} = 0. \tag{16}$$

This is easily accomplished numerically using the secant method, because the partial derivative has a simple analytical expression. This has been implemented in a function which calculates the minimum of $\Delta V(\theta)$. Next, this function is

passed as the argument of a robust minimization algorithm which does not require gradients (Brent's method [30]) and returns the optimum values of the true anomaly and impulse. The worst-case correction of the argument of the perigee over two years is 16°, of which 15° are due to orbital perturbations and 1° to the coupling with the Ω correction. This requires a maximum impulse ΔV_ω^I of 182 m/s, with the typical impulse being some 50% lower.

6.3.2. Low-thrust maneuver

Let the components of the acceleration **f** imparted by the motor be denoted with f_1, f_2 and f_3 in a radial-transverse-normal reference frame. It is possible to change ω while keeping the semimajor axis a and the eccentricity e constant, by applying the following in-plane acceleration over thrust arcs symmetric with respect to the perigee [28]:

$$f_1 = f\left(\frac{\cos E - e}{1 - e\cos E}\right) \tag{17}$$

$$f_2 = -f\left(\frac{\sqrt{1-e^2}\sin E}{1 - e\cos E}\right) \tag{18}$$

$$f_3 = 0 \tag{19}$$

Here E is the instantaneous value of the eccentric anomaly (which means the components of the acceleration vector change along the thrust arc). This acceleration causes a variation in ω

$$\Delta\omega = \frac{af\sqrt{1-e^2}}{GM_E e}\left(-3\bar{E} + 2e\sin\bar{E} + \frac{1}{2}\sin 2\bar{E}\right), \tag{20}$$

where $\bar{E}$ is the absolute value of the eccentric anomaly at either end point of the thrust arc. The length of the propelled arc is determined by the magnitude of the correction $\Delta\omega$ as shown in Fig. 10. The correction per orbit needed to compensate the worst-case perturbations is 0.0205°. Another 0.0014° must be added due to the coupling with the Ω maneuver (see Sect. 6.2.2) for a total of 0.022° per orbit. Note that the central part of the arc (i.e., the neighborhood of the perigee) is not available, as it is used for the ascending node correction. Therefore, the thrust arcs must be applied before and after the Ω correction

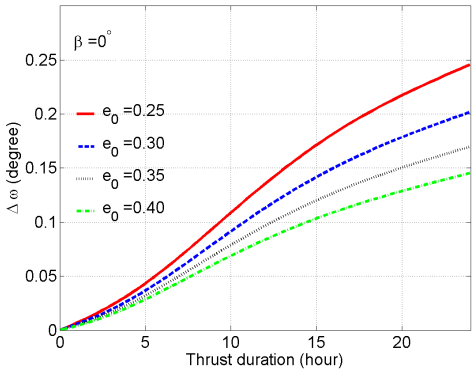

Figure 10: Change in ω per orbit achieved as a function of the eccentricity and total duration of the thrust arc. Thrust vector is in the orbital plane.

maneuver which, as shown in Sect. 6.2.2, lasts 4.2 hours. To determine the bounds of the thrust arcs, the value of $\Delta\omega$ for a duration of 4.2 hours is read from Fig. 10 (0.023°) and 0.022° are added obtaining 0.045°. The time corresponding to this value (7 hours) indicates the bounds of the thrust arcs. That is, the thrust arcs span 1.4 hours before and after the Ω correction (e.g., from 3.5 to 2.1 hours before perigee for the first arc). The associated impulse is 0.27 m/s per orbit, which amounts to a total ΔV_{ω}^{LT} of 200 m/s over two years.

6.4. Correction of the eccentricity

The change in eccentricity is due almost completely to the effect of the Moon. The variation over a two-year period is small and has no appreciable effect on the coverage footprint. Therefore, if left uncorrected it would not affect the primary mission of the satellites. However, due to operational reasons (e.g., to avoid interfering with the orbits of other spacecraft) it may be desirable to keep e constant. The impulsive maneuver required is thus included for reference purposes. The low-thrust option, on the other hand, has been disregarded because, according to [28, 31], in order for the maneuver not to affect the semimajor axis, thrust should be applied over the entire orbit, i.e., also around apogee when the satellite is online for communication service.

6.4.1. Impulsive maneuver

The maneuver consists in a pair of burns applied at the line of apsides. For example, to increase e the apogee is raised with a forward impulse at the perigee, while the perigee is lowered by the same amount with a reverse impulse at the apogee. For small corrections, the total impulse can be linearized as follows:

$$\Delta V = \frac{GM_E}{4a}\left(\frac{1}{V_\pi} + \frac{1}{V_\alpha}\right)\Delta e. \tag{21}$$

For a worst-case correction $\Delta e = 0.07$ (set 9, $\Omega_0 = 120°$) an impulse ΔV_e^I of 60 m/s is required.

6.5. Correction of the orbital inclination

The change in inclination is due almost entirely to the lunar perturbation. The variation is small and has little impact on the constellation coverage. Given that a change-of-plane maneuver requires a comparatively large impulse, it should be carefully evaluated whether this correction is strictly necessary. For the sake of completeness, the budget of the impulsive maneuver is included (Sect. 6.5.1). The low-thrust option, however, has been discarded on the following basis: in order for the maneuver to cause the maximum rate of change of i, thrust must be perpendicular to the orbit plane and must be applied over an arc centered at a point whose true anomaly (θ_i) depends on eccentricity (e) and argument of perigee (ω) [31]:

$$\sin(\theta_i + \omega) = -e\sin\omega. \tag{22}$$

For the orbits under consideration, such point falls in the northern hemisphere, i.e., in the part of the orbit reserved for telecommunication service.

6.5.1. Impulsive maneuver

A change Δi in the orbital inclination not affecting the position of the ascending node is achieved by an impulse applied at either node:

$$\Delta V = 2V\sin\left(\frac{\Delta i}{2}\right). \tag{23}$$

For a worst-case correction $\Delta i = 1.2°$ (set 1, $\Omega_0 = 300°$) an impulse ΔV_i^I of 62 m/s is required.

6.6. Estimation of total station-keeping cost

The worst-case scenario (set 9, $\Omega_0 = 180°$) for the most relevant maneuvers, i.e., Ω and ω correction, corresponds to velocity variations of 282 m/s ($= \Delta V_\Omega^I + \Delta V_\omega^I$), and 490 m/s ($= \Delta V_\Omega^{LT} + \Delta V_\omega^{LT}$), for the high and low thrust strategies, respectively. The perturbations of e and i for this scenario are 0.027 and 0.17°, respectively (observe these are not the worst-case values recorded in Table 2). The impulses required to correct these perturbations are $\Delta V_e^I = 23$ m/s for eccentricity and $\Delta V_i^I = 11$ m/s for inclination. Therefore, the total impulse budget over two years for the high-thrust maneuvers when all four parameters are corrected is $\Delta V = 316$ m/s.

7. End-of-life disposal

Once a satellite reaches the end of its operational life, measures must be taken to prevent it from interfering with the operation of active spacecraft. **Low-altitude satellites are often removed by the action of atmospheric drag. For the orbits under consideration in this paper, artificially de-orbiting the satellite to let it burn in the atmosphere is out of question due to the enormous impulse required ($\approx$ 1 km/s). On the other hand, allowing the natural orbital evolution to act may decrease significantly the de-orbiting cost. Recent studies show that the orbital instabilities due to the lunisolar perturbations and the associated resonances, produce an increase of the orbital eccentricity and may cause atmospheric reentry over medium to long time scales (from decades to hundreds of years) [32, 33, 34]. However, if left uncontrolled, a satellite in an inclined geosynchronous orbit quickly enters the GEO protected ring**. If this has to be avoided, a viable option is to move the spacecraft to a circular orbit far from the most congested bands (e.g., avoiding conflicts with GPS and GEO satellites) [35]. In this section we analyse the operational strategy and the cost associated to this type of disposal by considering both impulsive and continuous thrust maneuvers.

7.1. Impulsive disposal

The orbit can be circularized to an altitude intermediate between the perigee and apogee with a two-burn impulsive maneuver. For example, the maneuver could start with a backward impulse at the perigee followed by a forward burn at the apogee of the transfer orbit to circularize the trajectory. Alternatively, the maneuver could start with a forward burn at the apogee followed by a backward impulse at the perigee of the transfer orbit. It turns out that the best strategy is to start the transfer at the apogee of the original orbit. Fig. 11 shows the reduction in impulse achieved by starting the transfer at the apogee as a function of the radius of the final circular orbit (for an initial orbit eccentricity $e_0 = 0.4$). Note that when the radius of the final orbit is the same as the perigee or apogee of the initial orbit (25299 km or 59030 km respectively) the difference vanishes because the transfer becomes a single-burn maneuver. To determine the optimal disposal altitude, the total impulse requirement is plotted against the radius of the parking orbit, as shown in Fig. 12. It is clear from the plot that the cost is minimum when the radius of the parking orbit is equal to the initial apogee. Observe that the cost of disposal increases dramatically if the radius of the final orbit is higher than the initial apogee or lower than the initial perigee. Note also that, from the operational point of view, the optimum circular disposal orbit is perfectly viable, as it lies well above the GEO ring. Table 3 summarizes the cost of impulsive disposal for the different eccentricities tested. The cost increases with the initial eccentricity, with a maximum of 586 m/s for $e_0 = 0.4$.

Table 3: Cost (third column) of the impulsive disposal in a circular orbit at initial apogee altitude (second column). The first column gives the initial orbital eccentricity.

e_0	Disposal orbit radius (km)	Disposal cost (m/s)
0.25	52706	368
0.30	54814	440
0.35	56922	513
0.40	59030	586

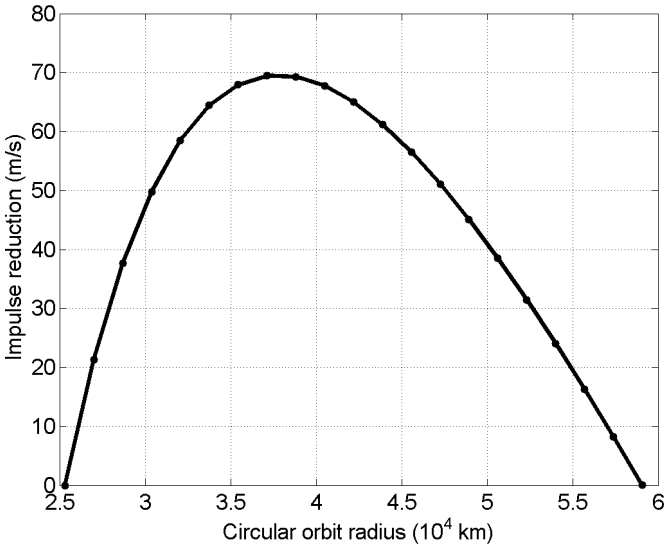

Figure 11: Reduction in impulse achieved by starting the disposal maneuver at the apogee instead of the perigee, as a function of the radius of the final circular orbit (for an initial orbit eccentricity $e = 0.4$).

7.2. Low-thrust disposal

Circularisation at apogee altitude can be obtained by continuous in-plane thrust. Results are here provided for a solution consisting in uninterrupted thrust perpendicular to the major axis of the orbit (see also [28] and [36]). Table 4 gives the performance of this maneuver for the four values of the initial eccentricity chosen. The disposal of the most eccentric orbit ($e = 0.4$) takes 344 days and corresponds to a velocity variation of 780 m/s.

8. Conclusions

A study of orbital evolution, station-keeping maneuvers and disposal options for telecommunications satellites in highly-inclined geosynchronous orbits has been presented. A numerical model of the rel-

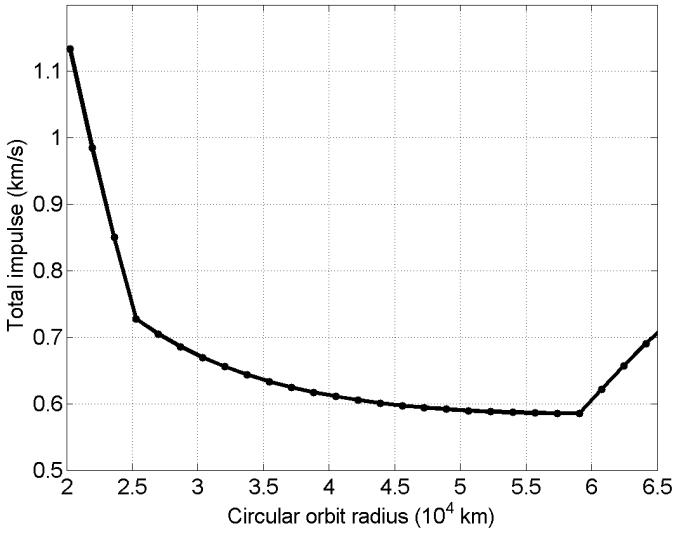

Figure 12: Impulsive disposal in a circular orbit: total impulse requirement against the radius of the final orbit ($e_0 = 0.4$).

evant physical effects has been developed which, considering the accuracy requirements of the mission and the instantaneous satellite altitude, dynamically adjusts the expansion degree of Earth's gravitational field to obtain maximum performance during orbit propagation. The model is applied to nine sets of constellations (defined by orbital inclination and eccentricity) that serve areas of maximum economic viability (i.e., housing the largest population). A station-keeping strategy has been devised where, instead of keeping the orbital elements constant, only the ground track of the constellation is maintained while reducing the propellant expense. The impulse budget for Ω corrections can thus be reduced by as much as 90%.

The results show that, due to the high altitude of the perigee, the most important perturbation is due to the Moon with the harmonics of the gravitational field of the Earth playing a minor role. The magnitude of the Lunar perturbation depends strongly on the rela-

Table 4: Characteristics (i.e., execution time and cost) of the low-thrust disposal in a circular orbit at initial apogee altitude assuming uninterrupted in-plane thrust perpendicular to the major axis of the orbit.

e_0	Execution time (days)	Disposal cost (m/s)
0.25	217	490
0.30	259	590
0.35	301	680
0.40	344	780

tive inclination of the orbital planes of the satellite and Moon, which is a function of the separation of their ascending nodes. Therefore, the three satellites of a constellation experience vastly different evolutions at any given time as their orbital planes are offset by 120 degrees. Note that, due to the dominance of Lunar perturbations and the precession of Moon's orbit, the behavior of a satellite at an epoch different from that chosen in the discussion (01/07/2013) can be roughly approximated by a shift in Ω equal to the motion of Lunar ascending node. Thus, the data presented are also indicative of the evolution of spacecraft with arbitrary launch dates.

To provide an upper bound of the station-keeping cost, a worst-case scenario (requiring the maximum impulse over a two-year period) has been identified. For the sake of completeness, typical (i.e. representative of the median value) changes of orbital elements are also provided. The impulse budget has been computed for high and low-thrust maneuvers. The impulsive correction of the argument of the perigee uses an elliptical transfer arc which minimizes the propellant consumption. As there is no closed expression for the parameters of the optimum transfer ellipse, an efficient solution has been found using a combination of minimization algorithms with and without gradients. For the impulse strategy, the worst-case scenario requires

a total impulse of 316 m/s. This includes 182 m/s for ω corrections and 100 m/s for Ω, with eccentricity an inclination accounting for around 10% of the total budget. The low-thrust maneuvers, for their part, have ΔV requirements that are roughly twice as large.

From the economic point of view, the combination of orbital parameters yielding the minimum station-keeping cost is extremely interesting. The fact that each constellation includes three different orbital planes subject to vastly different lunar perturbations (which also change in time due to the precession of Moon's orbit) means that there is no single set of optimum orbital parameters. However, it is possible to find families of orbits that, over time, experience smaller-than-average changes of the orbital elements. The largest slice of the propellant budget (almost 60%) corresponds to ω corrections, offering the maximum potential for cost reduction. Among the different sets analyzed, orbits with e_0=0.25 and 55 degrees of inclination experience the slowest drift of the perigee.

Finally, an end-of-life disposal strategy has been outlined. Given the high altitude of the perigee, lowering it to the point where atmospheric drag de-orbits the satellite in a reasonable timeframe is unfeasible (i.e., needs an impulse close to 1 km/s). Instead the spacecraft is parked in a circular orbit far from operational satellites. Analysis shows a minimum impulse requirement when the radius of the circular orbit coincides with the apogee of the initial orbit. Cost of disposal increases with the eccentricity of the orbit. For impulsive maneuvers 586 m/s are needed for e_0=0.4. The orbit can alternatively be circularized with in-plane low-thrust perpendicular to the major axis at a cost of 780 m/s (the maneuver taking almost a year to complete).

References

[1] C. E. Fossa, R. Raines, G. Gunsch, et al., An overview of the IRIDIUM (R) Low Earth Orbit (LEO) satellite system, Proceedings of the IEEE 1998 National Aerospace and Electronics Conference, NAECON, 1998, pp. 152–159.

[2] Y. F. Kolyuka, N. M. Ivanov, T. I. Afanasieva, et al., Examination of the lifetime, evolution and re-entry features for the "Molniya" type orbits, Proceedings of the 21st International Symposium on Space Flight Dynamics — 21st ISSFD, Toulouse, France, 2009.

[3] M. J. Bruno, H. J. Pernicka, Tundra constellation design and station-keeping, Journal of Spacecraft and Rockets 42 (5) (2005) 902–912. doi:10.2514/1.7765.

[4] V. Boccia, M. Grassi, M. Marcozzi, et al., Mission Analysis and Orbit Control Strategy for a Space Mission on a Polar Tundra Orbit, Proceedings of the 63rd International Astronautical Congress, Naples, Italy, 2012, IAC-12-C1.4.7.

[5] L. Loge, Arctic communications system utilizing satellites in highly elliptical orbits, Ph.D. thesis, Norwegian University of Science and Technology (2013).

[6] J. R. Wertz, Coverage, Responsiveness and Accessibility for Various "Responsive Orbits", Proceedings of the 3rd Responsive Space Conference, Los Angeles, CA, 2005.

[7] G. Cavallaro, D. Phan-Minh, M. Bousquet, HEO Constellation Design for Tactical Communications, First AESS European Conference on Satellite Telecommunications (ESTEL), Rome, Italy, 2012.

[8] P. Anderson, M. MacDonald, B. Dobke, A geostationary equivalent polar observation system, Proceedings of the 12^{th} Reinventing Space Conference, London, United Kingdom, 2014, BIS-RS-2014-22.

[9] G. D. Krebs, Sirius FM1, FM2, FM3, FM4 (Radiosat 1, 2, 3, 4), http://space.skyrocket.de/doc_sdat/sirius-cdr.htm, accessed: 2017-04-04.

[10] S. S. Loral, Ssl homepage, http://www.sslmda.com/, accessed: 2017-04-04.

[11] E. Fantino, R. Flores, A. Di Salvo, et al., Analysis of Perturbations and Station-Keeping Requirements in Highly-Inclined Geosynchronous Orbits, Proceedings of the 25^{th} International Symposium on Space Flight Dynamics, ISSFD October 19 - 23, 2015, Munich (Germany), 2015.

[12] A. C. Andersen, Interactive map of world population by point, latitude, and longitude, http://blog.andersen.im/2013/05/interactive-map-of-world-population-by-point-latitude-and-longitude/, accessed: 2017-04-04 (2013-05-10).

[13] D. Balk, U. Deichmann, G. Yetman, ISLSCP II Global Population of the World. In: Hall, Forrest G., G. Collatz, B. Meeson, S. Los, E. Brown de Colstoun, and D. Landis (eds.) ISLSCP Initiative II Collection. Data set, Oak Ridge National Laboratory Distributed Active Archive Center, Oak Ridge, TN, 2010, doi: 10.3334/ORNLDAAC/975.

[14] O. Montenbruck, G. E., Satellite Orbits: Models, Methods and Applications, Springer, Berlin, Germany, 2000, ISBN: 3-540-67280-X.

[15] E. M. Standish, Keplerian elements for approximate positions of the major planets, http://ssd.jpl.nasa.gov/txt/aprx_pos_planets.pdf, accessed: 2017-03-07.

[16] E. M. Standish, Planetary satellite mean orbital parameters, http://ssd.jpl.nasa.gov/?sat_elem, accessed: 2017-03-07.

[17] R. Fitzpatrick, An Introduction to Celestial Mechanics, Cambridge University Press, 2012, ISBN: 978-1107023819.

[18] W. Heiskanen, H. Moritz, Physical Geodesy, Freeman, San Francisco, CA, 1967, ISBN: 978-0716702337.

[19] S. Pines, Uniform representation of the gravitational potential and its derivatives, AIAA Journal 11 (1973) 1508–1511. doi:10.2514/3.50619.

[20] G. Balmino, J.-P. Barriot, N. Valès, Non-singular formulation of the gravity vector and gravity gradient tensor in spherical harmonics, Manuscripta Geodetica 15 (1) (1990) 11–16.

[21] G. Balmino, J.-P. Barriot, B. Koop, et al., Simulation of gravity gradients: a comparison study, Bulletin Géodesique 65 (4) (1991) 218–229. doi:10.1007/BF00807265.

[22] E. Fantino, S. Casotto, Methods of harmonic synthesis for global geopotential models and their first-, second- and third-order gradients, Journal of Geodesy 83 (4) (2009) 595–619. doi:10.1007/s00190-008-0275-0.

[23] S. Casotto, E. Fantino, Gravitational gradients by tensor analysis with application to spherical coordinates, Journal of Geodesy 83 (7) (2009) 621–634. doi:10.1007/s00190-008-0276-z.

[24] N. K. Pavlis, S. A. Holmes, S. C. Kenyon, et al., The development and evaluation of the Earth Gravitational Model 2008 (EGM2008), Journal of Geophysical Research 117 (B4). doi:10.1029/2011JB008916/.

[25] J. M. A. Danby, Fundamentals of Celestial Mechanics, Willmann-Bell, Richmond, VA, 1992, ISBN: 0-943396-20-4.

[26] S. Franchini, O. López García, Introducción a la Ingeniería Aeroespacial, Editorial Garceta, Madrid, Spain, 2011, ISBN: 978-8492812905.

[27] V. A. Chobotov, Orbital mechanics, American Institute of Aeronautics and Astronautics, Reston, VA, 2002, ISBN: 978-1563475375.

[28] J. Pollard, Simplified analysis of low-thrust orbital maneuvers, Tech. Rep. TR-2000 (8565)-10, Aerospace Corporation, El Segundo, CA (2000).

[29] D. F. Lawden, Impulsive Transfer Between Elliptical Orbits, in: Optimization Techniques, with Applications to Aerospace Systems, Leitmann G. (ed.), Academic, New York, NY, 1962, ISBN: 978-0124429505.

[30] R. P. Brent, An Algorithm with Guaranteed Convergence for Finding a Zero of a Function, in: Algorithms for Minimization without Derivatives, Prentice-Hall, Englewood Cliffs, NJ, 1973, ISBN: 0-13-022335-2.

[31] A. Ruggiero, P. Pergola, S. Marcuccio, et al., Low-thrust maneuvers for the efficient correction of orbital elements, Proceedings of the 32^{nd} International Electric Propulsion Conference, Wiesbaden, Germany, 2011.

[32] J. Tang, X. Hou, L. Liu, Long-term evolution of the inclined geosynchronous orbit in Beidou Navigation Satellite System, Advances in Space Research 59 (2017) 762–774. doi:10.1016/j.asr.2016.07.012.

[33] A. B. Jenkin, J. P. Mcvey, J. R. Wilson, et al., Tundra Disposal Orbit Study, Proceedings of the 7^{th} European Conference on Space Debris, April 18 - 21, 2017, Darmstadt (Germany), 2017.

[34] C. Colombo, I. Gkolias, Analysis of Orbit Stability in the Geosynchronous Region for End-of-Life Disposal, Proceedings of the 7^{th} European Conference on Space Debris, April 18 - 21, 2017, Darmstadt (Germany), 2017.

[35] B. Kemper, Deorbiting a spacecraft from a highly inclined elliptical orbit, US Patent 2012/0119034 A1 (2012).

[36] E. Cabot, Study of end-of-life disposal options for highly-inclined geosynchronous satellites, Terrassa School of Industrial, Aeronautical and Audiovisual Engineering, Polytechnic University of Catalonia, Bachelor Dissertation (2016).